# Reversible doping and photo patterning of polymer nanowires

Zaira I. Bedolla-Valdez[1], Rui Xiao[2], Camila Cendra[3], Alice S. Fergerson[1], Zekun Chen[1], Alberto Salleo[3], Dong Yu[2], and Adam J. Moulé*[1]

[1]Department of Chemical Engineering, University of California Davis, Davis, California, USA.
[2]Department of Physics, University of California Davis, Davis, California, USA.
[3]Department of Materials Science, Stanford University, Palo Alto, California, USA

## Abstract

*Recent development of dopant induced solubility control (DISC) patterning of polymer semiconductors has enabled direct-write optical patterning of poly-3-hexylthiophene (P3HT) with diffraction limited resolution. Here we apply the optical DISC patterning technique to the most simple circuit element, a wire. We demonstrate optical patterning of P3HT and P3HT doped with the molecular dopant 2,3,5,6-Tetrafluoro-7,7,8,8-tetracyanoquinodimethane (F4TCNQ) wires with dimensions of 20-70 nm thickness, 200-900 nm width, and 40 μm length. In addition, we demonstrate optical patterning of wire patterns like "L" bends and "T" junctions without changing the diameter or thickness of the wires at the junctions. The wires themselves show up to 0.034 S/cm conductance when sequentially doped. We also demonstrate that a P3HT nanowire can be doped, de-doped, and re-doped from solution without changing the dimension of the wire. The combined abilities to optically pattern and reversibly dope a polymer semiconductor represents a full suite of patterning steps equivalent to photolithography for inorganic semiconductors.*

## 1 Introduction

Organic semiconductors (OSCs) are increasingly being included in optoelectronic devices in high value products like smartphones. The two strongest arguments for the use of OSCs are (1) that OSCs can be infinitely chemically tailored for different applications and (2) that they can, in principle, be solution-processed over large areas at low cost. These solution coating techniques have already been used to print optical devices like waveguides, light couplers, lasing media, photonic crystals, spectral filters, reflectors, and sensing devices[1] as well as printed electronic devices like thin-film transistors (TFTs), organic inverters, ring oscillators, logic gates, organic photovoltaics (OPVs), organic light emitting diodes (OLEDs) for display, OLED lighting, electronics components, and integrated smart systems.[1–5] Unfortunately, the application of argument (1) "infinite chemical tailorability" makes argument (2) "low–cost solution coating" much more challenging because each new material has to be re-optimized for coating or re-synthesized for photo cross-linking and many materials are just difficult or impossible to reproducibly synthesize and process.

The optoelectronic material properties of OSC materials are sufficient for industrial products, but there is no universally applicable approach or method for depositing, patterning, and doping OSC materials that serves the equivalent functions that photolithography does for silicon technology. For Si, a simple photolithography processing step defines a pattern on the substrate with diffraction limited resolution. We note that multi-step photolithography, e-beam, and other processes can produce significantly smaller features. Regardless of the photomask resolution, the mask enables selective area implantation of dopants into the Si, deposition of another material onto the Si, or etching the Si. Photolithography enables non-contact selective area patterning, etching, and doping with diffraction limited lateral resolution in Si. After Si processing, the lithographic mask is etched away without damaging the Si. Except in very limited cases, photolithography is not compatible with OSC processing because OSCs are damaged by removal of the mask and the other chemical processing steps. There is no fast and easy photopatterning method for OSCs that serves the same functions that photolithography serves for Si technology. The absence of an equivalent photoprocessing method with sub-micron resolution for OSC materials greatly limits the use of OSC materials in devices.

We present here a photoprocessing method that enables non-contact selected area patterning, etching, and doping of the organic semiconductor poly-3-hexylthiophene (P3HT) with diffraction limited lateral resolution. Diffraction limited resolution with a 405 nm laser yields well defined lateral features as small as 300 nm.[6] Compared to solution coating methods, for example inkjet printing, our method represents a $\sim$100$\times$ linear reduction in feature size, which is ideal for new applications in display, optics, and thin-film electronics. The ultra small features needed for microprocessing in Si are not needed for OSC technologies.

The optical processing steps are carried out in a geometry that is compatible with confocal optics. The pattern write speed and resolution is thus dependent on the quality and write speed of the photolithography tool. Diffraction limited resolution pattering has already been demonstrated.[6] Here we demonstrate the combined use of direct–

write dopant induced solubility control (DISC) patterning,[6] polymer doping using sequential solution processing,[7], and dopant removal using sequential chemical processing.[8] Using these processing steps sequentially, we fabricate nanowires of P3HT with dimensions of 20-70 nm thickness, 200-900 nm width, and 40 $\mu m$ length. Because the pattern is written using a laser, the nanowires can be written into wire geometries including "L" bends and "T" junctions without changing the wire diameter or thickness at the junctions. Using sequential solution processing steps to controllably dope and dedope the P3HT wire with the molecular dopant 2,3,5,6-Tetrafluoro-7,7,8,8-tetracyanoquinodimethane (F4TCNQ) demonstrates that both doped and intrinsic nanoscale domains can be easily made from solution processing. The reversible doping of conjugated polymers for electrochemical applications has gained enormous recent interest and the use of patterning, as demonstrated here, could enable numerous device applications in organic electrochemical transistors (OECTs) and or bio organic electronic applications.[9,10]

To support and qualify our assertion that the combined use of optical patterning and doping techniques presented here constitutes a qualitative and quantitative improvement over previously presented techniques for patterning OSCs, we critically review the most well cited and respected review articles on various patterning methods for OSCs. We then present the patterning and de-doping of P3HT nanowires and discuss our results in the context of competing optical patterning and doping techniques.

## 2 OSC nano/micro patterning review

**Large area coating methods:** A review of roll-to-roll (R2R) compatible printing techniques for coating organic semiconductors onto flexible substrates includes screen printing, spray coating, inkjet printing, gravure coating, doctor blade coating, and slot-die coating. All of these techniques are mature technologies that enable printing over large areas quickly onto flexible substrates. Screen printing, inkjet printing, and gravure printing have the added advantage that they can enable lateral patterning with reliable resolution of 50 $\mu m$ and maximum resolution of 10-20 $\mu m$ through microfluidic control of droplet size, viscosity, and drying rate.[11–13] The printing/coating speed can be improved using ancillary processing for example with lasers, vapor deposition, or combined use of complimentary techniques.[11] Inclusion of nanoparticles into ink solutions, selective dissolution, substrate patterning, and the intelligent use of microfluidic forces at interfaces enable the formation of highly organized substructures that constitute patterning order that is much smaller than the minimum feature size that can be achieved directly through coating techniques.[14]

**High resolution contact printing:** Microcontact and nano-imprint coating uses a hard material mask to imprint or mold a pattern into a polymer. With these techniques, making a transfer mold is difficult, as is keeping the mold from becoming fouled from repeated use.[1] However, these techniques yield a gain in pattern resolution to 1-20 $\mu m$. Finally, transfer contact printing employs a pre-made PDMS stamp to pick up a material pattern from one film and then transfer the material pattern to a different substrate. Pressure changes are used to adhere the film material to the PDMS stamp for lift off. For transfer of the film pattern, the material must adhere to the new substrate while the PDMS stamp is stretched and flexed to separate the stamp from the transferred material. Transferred metal and Si ribbons have been deposited with resolution of $\sim$100 nm[11,15] but in a R2R setting the highest reported resolution is $\sim$10 $\mu m$.[11,15]

Polymer nanostructures are difficult to print using transfer contact printing because the mechanical properties of the polymer semiconductor are much closer to those of the PDMS stamp than of the substrates, metals or Si, leading to transfer constraints such as pattern distortion near an edge, limited lifetime of the mold, residue after patterning, and difficulty in alignment (it is not possible to see through the mold to align the transferred material).[13,15,16] For contact and transfer printing techniques, the molded material can be composed of a composite of smaller particles, for example Ag nanowires in a matrix material. The use of microfluidic forces or mechanical strain can be used to align or order the nanoparticles during transfer fabrication to achieve ordered patterns, aligned Ag nanowires (1-100 nm) within patterned circuits (0.1-10 $\mu m$) or heirarchical order.[14,17]

For all of the listed printing methods there is a tradeoff between printing speed and print resolution, thus the task of achieving sub-$\mu m$ features over large areas (in the order of $\sim$m$^2$) remains a significant challenge. All of the listed printing techniques have been used to fabricate transparent conducting layers, in devices such as organic photovoltaics (OPVs), organic light emitting diodes (OLEDs), organic field effect transistors (OFETs), waveguides, lasers, touch panels, and strain sensors.[12,13,16,18]

**Extrusion Methods:** Inkjet printing is the most developed direct–write patterning method.[5] Printed electronics based on inkjet technology can be fabricated with mid-level resolution of 10's of $\mu m$ and speed 0.01-1 m$^2$/s. One of the main issues for inkjet printed electronics is the "coffee stain effect" where the fluid in a droplet is pulled to the outside to form a ring due to the increased evaporation speed at the edge of the droplet.[19]

Direct extrusion methods like electrospinning have the ability to generate polymer wires with diameter below 1 $\mu m$ but usually the wire whips around as it extrudes so only mats of fibers can be used.[16] In most applications, the electronic material is a metal or inorganic nanomaterial that is in a emulsion of a printable polymer to make an electronic material that can flow.[20,21] Electrohydrodynamic organic nanowire printing has demonstrated directional fabrication of extruded nanowires of conjugated polymers such as P3HT and N2200 mixed with PEO with a diameter of only 300 nm. This technique even led to fabrication of functioning single nanowire P3HT transistors as well as inverters based on P3HT for p-type and N2200 for n-type channels.[22] The only disadvantage of electrohydrodynamic organic printing is the need to mix OSC polymers with a low

glass transition temperature ($T_g$) polymer like polyethylene oxide (PEO) that allows the OSC polymer to flow.

**Photo cross-link methods:** Photo-induced cross-linking methods to pattern OSCs are the most powerful existing methods to directly write OSC materials. Based on reactions originally developed for photoresists, conjugated polymers or small molecule OSCs can be decorated with cross-linkable groups that will react only with exposure to light. These light induced reactions can link reactive sites on side chains to render the material completely insoluble after exposure.[23] For device applications, photo cross-link reactions must be specific. If a linker molecule can react with any site, conjugated bonds are broken or radical reactions started that result in material property degradation. Even for side chain specific reactions, the reactive site changes the packing of the polymer, which reduces the optoelectronic performance or crystalline materials. The optoelectronic properties of cross-linked amorphous small molecule OSCs are nearly identical to films that are not cross-linked.[23,24]

A related approach is to fabricate devices with a series of polymer layers that are only soluble in orthogonal solvents.[25,26] This system does allow near diffraction limited deposition of multiple materials provided that solvent orthogonality can be maintained, which limits the device to three sets of materials soluble in aqueous, non-polar, and fluorinated solvents. It also requires synthesis of materials with optimal properties but solubility in three different solvent systems.

While there are many examples of successful applications of orthogonal solvent processing and photo cross-link reactions in organic electronics, no single method is able to become universal. For each separate process, a large amount of synthetic effort is needed to synthesize cross-linkable molecules. Photo cross-linkable molecules are highly reactive and often must be transported and deposited in $H_2O$, $O_2$, and light free environments. The expense of synthesizing and fabricating devices with cross-linkable molecules is high and requires a large chemical processing infrastructure. A further problem is that new molecules, architectures, and devices cannot be cheaply tested due to the large infrastructure needed. Thus the challenges to develop applications using photo cross-link methods are in most senses not scientific but economic/practical.

**Polymer nanowire growth methods:** In general, organic nanowires are fabricated using solution self assembly of crystalline nanowires or amorphous nanoparticles followed by deposition of the preformed nanoparticles in a matrix of some other organic filler to form a composite material. For example, graphene flakes or carbon nanotubes in a polymer filler form a composite material that is flexible, conductive, and solution processable.[21] Alternatively, the nanoparticle solutions can be diluted to allow study of the material properties of individual nanowires.[17] While it is possible to study individual nanowires, manipulating individual carbon nanowires for use in devices, like transistors, or for conductivity measurements, is exceedingly difficult because of their small size, delicacy, and because each particle must be moved individually. Conjugated small molecule or polymer nanowire lateral dimensions of $<10$ nm with lengths of over 100 nm are commonly reported.[13,16,17] So while molecular self assembly yields the smallest nanowires, they are in general delicate and prohibitively difficult to pattern into useful sensors and circuit elements.[21] Organic nanowires have also been directionally crystallized in a $Al_2O_3$ nanoporous molds and released using selective etching.[16]

# 3 Results and discussion

The P3HT nanowire samples were prepared using the same light induced patterning technique presented previously.[6] For each step in the fabrication process, a UV/vis/NIR spectrum was taken and is depicted in Figure 1a, a grazing-incidence wide-angle X-ray scattering (GIWAXS) 2D pattern was acquired (full data set in Supporting Information Figure S2) with out-of-plane and in-plane lineouts shown in Figure 1b, and an AFM image was collected and is shown in Supporting Information Figures S3 and S4. In a first step, a P3HT film was spin coated from Sigma-Aldrich electronic grade P3HT dissolved in a chlorobenzene (CB) solution onto a microscope coverslip with a total thickness of $\sim$60 nm. The UV/vis/NIR shows a typical P3HT absorbance spectrum and the AFM image shows a fairly flat, featureless surface with a RMS roughness of $1.9\pm0.1$ nm as is typical for an unannealed film. The GIWAXS 2D pattern of as-cast P3HT presents a predominant edge-on texture, with a lamellar distance of $16.3\pm0.6$ Å and a $\pi$-stacking distance of 3.85 Å, which is consistent with published research.[27] Lamellar (100) and $\pi$-stacking (010) distances were extracted from fitting the diffracted peak positions in the out-of-plane and in-plane directions, respectively.

In a second step, F4TCNQ with a concentration of 0.1 mg/ml in acetonitrile (AN) was spin coated on top of the dried P3HT film, yielding a sequentially doped P3HT/F4TCNQ film.[7] The UV/vis/NIR shows decreased absorbance for neutral P3HT and increased absorbance at $\sim$400 nm, $\sim$750 nm and $\sim$850 nm for $F4TCNQ^-$ and increased absorbance at 700-950 nm and $>1500$ nm for $P3HT^+$. These spectral changes are identical to the typically reported changes when doping P3HT with F4TCNQ.[28] The AFM of the sequentially doped film is equally featureless and has a statistically identical RMS roughness of $1.8\pm0.1$ nm. The RMS roughness results shows that the film morphology does not change, within our measuring ability, with sequential doping. However, the GIWAXS data shows a clear increase in the lamellar spacing to $18.0\pm0.6$ Å and the $\pi$-stacking is reduced to 3.7 Å. De-doping of a sequentially doped film using 1:10 1-aminobutane:acetone destroys the F4TCNQ molecules and returns a quantitatively undoped P3HT film.[8] The UV/vis/NIR spectrum of the de-doped film shows identical absorbance across the entire spectrum to the as-cast P3HT film. Comparison of the GIWAXS patterns from as-cast and de-doped films shows no discernable differences in the structure and packing of the crystallites, as shown in Figure 1b. Indeed, the extracted lattice spacings of the de-doped film are identical to the as-cast P3HT film

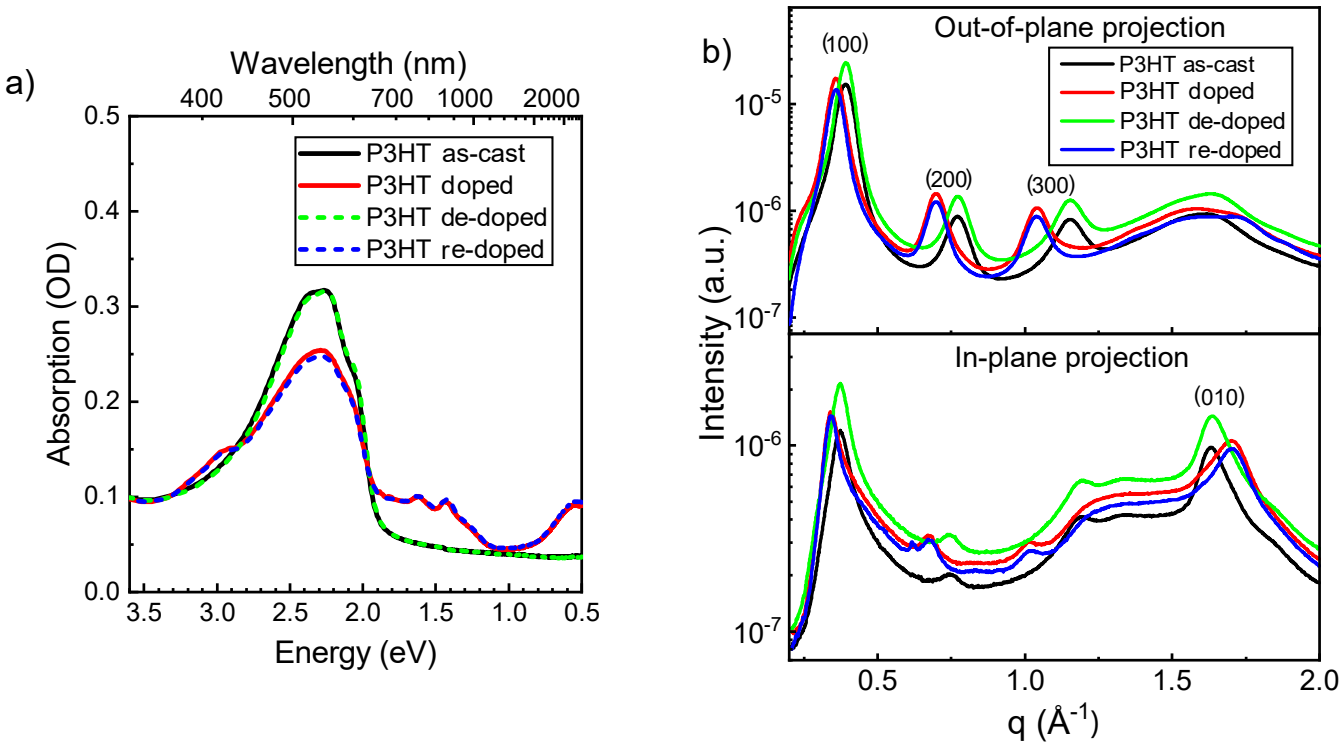


**Figure 1** *a) Normalized UV/vis/NIR spectra of a high $M_W$ and highly regio-regular as-cast P3HT film (—), that is sequentially doped with AN:F4TCNQ solution (—), sequentially de-doped by dipping into a 1:10 1-aminobutane:acetone solution (- - -) and sequentially re-doped from an AN:F4TCNQ solution (- - -). All spectra were taken of the same film on a glass substrate. This same film was used for the images in Figure 4, S3 and S4. b) Out-of-plane (top) and in-plane projections (bottom) of 2D GIWAXS data for an as-cast P3HT film (—), doped P3HT film (—), de-doped P3HT film (—) and re-doped P3HT film (—). Four separate films were used for the GIWAXS data on Si substrates, so the UV/vis/NIR and GIWAXS data was identically prepared, but the data does not all come from the same film.*

(16.3±0.6 Å and 3.85 Å for the lamellar and $\pi$-stacking distances, respectively). Finally, the de-doped films was again sequentially doped with a concentration of 0.1 mg/ml F4TCNQ in acetonitrile (AN). The structure and packing of the crystallites in the sequentially doped and re-doped P3HT are identical (Figure 1b), proving that P3HT films can be reliably and repeatedly doped from solution.

The lattice changes are consistent with previously published literature on sequential doping of P3HT with F4TCNQ, in which the F4TCNQ is reported to intercalate into the side chains of P3HT crystalline domains.[27,29] However, we had previously reported that sequential doping of F4TCNQ from AN into P3HT resulted in deposition of the F4TCNQ in the amorphous domains of P3HT and no intercalation into the crystallites.[7,30] Clearly something about the two studies is different.

After some analysis, we determined that there are only two possible and linked explanations to explain insertion of F4TCNQ into P3HT crystals in some samples and not others. The first explanation is that the $T_g$ of P3HT is just below room temperature[31,32] and so very small differences in the temperature at which F4TCNQ is added to P3HT in the vapor phase or using an orthogonal solvent will affect whether the P3HT crystallites can be deformed enough to enable intercalation of the F4TCNQ. In our case, we realized that there could be significant differences in the sample temperature history in the 2-3 hour drive from Davis to the Stanford Linear Accelerator Center (SLAC) depending on variables like outdoor temperature. These small variations in sample temperature during or directly after sequential deposition are enough to induce intercalation of the F4TCNQ into P3HT crystals. The second related issue is that the $T_g$ of P3HT depends on the molecular weight ($M_W$), polydispersity, and regio-regularity, which varies widely between batches even from the same vendor.[33] Since our previous data shows that F4TCNQ could not enter crystalline P3HT domains with sequential doping[7] and our current data clearly shows that F4TCNQ does enter crystalline P3HT domains and changes the lattice spacing, it is clear that our new sample of P3HT has lower $M_W$ and/or regio-regularity and/or was processed at a warmer temperature than the previous sample. Also, if the $M_W$ or regio-regularity is lower, then the $T_g$ will also occur at a lower temperature.[33] To further highlight the issue that can occur when switching polymer batches with similar $M_W$ but different regioregularity and PDI, we show a still lower quality P3HT sample in which the sample looses volume with sequential processing (supporting information Figure S5). This was the sample used for the wire studied in Figure 3. The low $M_W$ and low regioregular P3HT chains are dissolved from the film whereas with a higher $M_W$ and higher regioregular sample and identical solvents, the higher $M_W$ and regioregular film does not dissolve at all as seen in Figure 1a.

After sequential coating and doping steps, the P3HT/F4TCNQ film is sealed into a sample cell as depicted in Figure 2a. In contrast to our previous publications in which we used tetrahydrofuran (THF) for patterning P3HT,[6,34] here we used 2-Methyltetrahydrofuran (mTHF) for the dissolution solvent because it is less volatile but still undergoes the de-doping reaction with optically excited F4TCNQ described previously.[35] The sample cell geometry enables optical excitation with a laser scanning confocal microscope (LSCM) and a highly focused spot size of ~500 nm diameter with 405 nm light. Figure 2b shows a blow-up of the sample during optical excitation where the focused laser power excites the photo de-doping reaction in a limited volume. As the de-doping reaction occurs, the P3HT regains solubility and is completely dissolved in less than 100 $\mu s$ per pixel (focused illuminated area = 500 nm dia spot for this image) in this instrument.[6] With high intensity laser excitation at 405 nm, the dissolution occurs due to a combination of two mechanisms. First the 405 nm light excites the F4TCNQ and the excited state of F4TCNQ reacts with mTHF to form a non-doping and soluble spectator molecule.[35] As the F4TCNQ reacts, the P3HT is de-doped and regains solubility. The second mechanism occurs from photothermal heating of the film by the laser, which causes subsequent dissolution via increased solubility at higher temperatures. Exciting with high intensity 405 nm light causes both mechanisms to be active. Our fastest recorded dissolution times are ~1$\mu s$ per pixel, which is near the limit of mass transport by a fluid over the appropriate volume.[36] Figure 2d depicts a fluorescence image of a completed de-doped nanowire. The P3HT/F4TCNQ film was removed from the vicinity of the electrodes and between them to define a direct–write nanowire. Although the write speed per/pixel is very rapid, the area write speed is slow due to the high focus (small area) of the write-beam. This is why we left much P3HT material in place that is further from the wire.

Over >10 trials we made a series of nanowire samples with thickness of 20-60 nm, average width of 300-800 nm and length of 40-50 $\mu m$, which was set by the distance between electrodes. For many of the wires, we could not record AFM, KPFM, UV/vis/NIR and conductivity measurements on the same wire sample (due to air exposure usually), so we included only the two most complete data sets here. We found that for some samples the film thickness was the same before and after patterning as was the case for the sample in Figure 1, while for other samples the film was thinner after patterning. We determined the batch of P3HT is very important. P3HT chains that have lower $M_W$ or regioregularity are more soluble and thus can be removed from even a doped film. To demonstrate the differences between P3HT batches, we show UV/vis/NIR for doped, de-doped, and re-doped films for two different P3HT samples fabricated using different polymer batches (supporting information Figure S5). In the first low PDI sample, no polymer is dissolved and the film maintains its thickness. For higher PDI sample, the chains are fractionated by a marginal solvent. This result is consistent with a recently published paper on additive DISC pattering.[37]

In order to evaluate the electronic properties of the P3HT nanowire devices, we measured current-voltage (I-V) curves

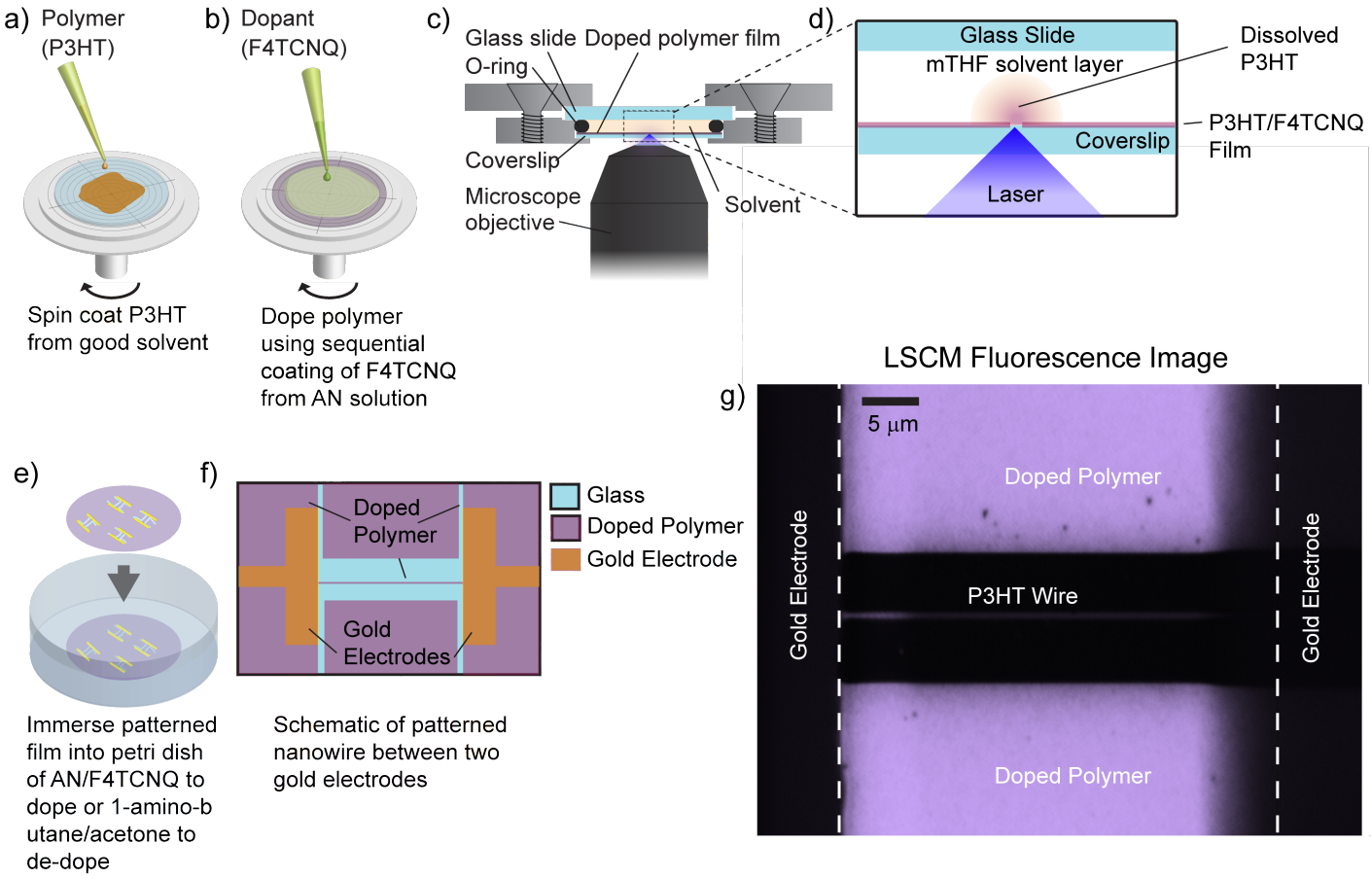


**Figure 2** *Schematic of wire fabrication process and completed wire: a) First the P3HT is spin coated onto a glass coverslip with pre-fabricated gold electrodes. b) Next the film is doped using sequential spin coating of F4TCNQ from an AN solution. c) The coverslip is then sealed into a sample holder that traps a solvent layer over the film. An LSCM is used to illuminate the film through the glass coverslip. d) A blow up of the boxed region shows the dissolution process where a LSCM laser dissolves dissolves the P3HT/F4TCNQ into the solvent only where the laser is focused. e) After patterning, the doping level is increased by immersing in a AN/F4TCNQ solution. The dopant is completely removed by immersing in a 1:10 1-aminobutane/acetone solution. f) Depicts a schematic of the film where gold electrodes are first deposited onto the coverslip followed by the P3HT/F4TCNQ film. Wires are fabricated by removing all of the material between and next to the electrodes via illumination to re-expose the glass. d) LCSM fluorescence image of a neutral P3HT nanowire between gold electrodes. The electrodes are dark because they block the laser. The nanowire spans the two electrodes.*

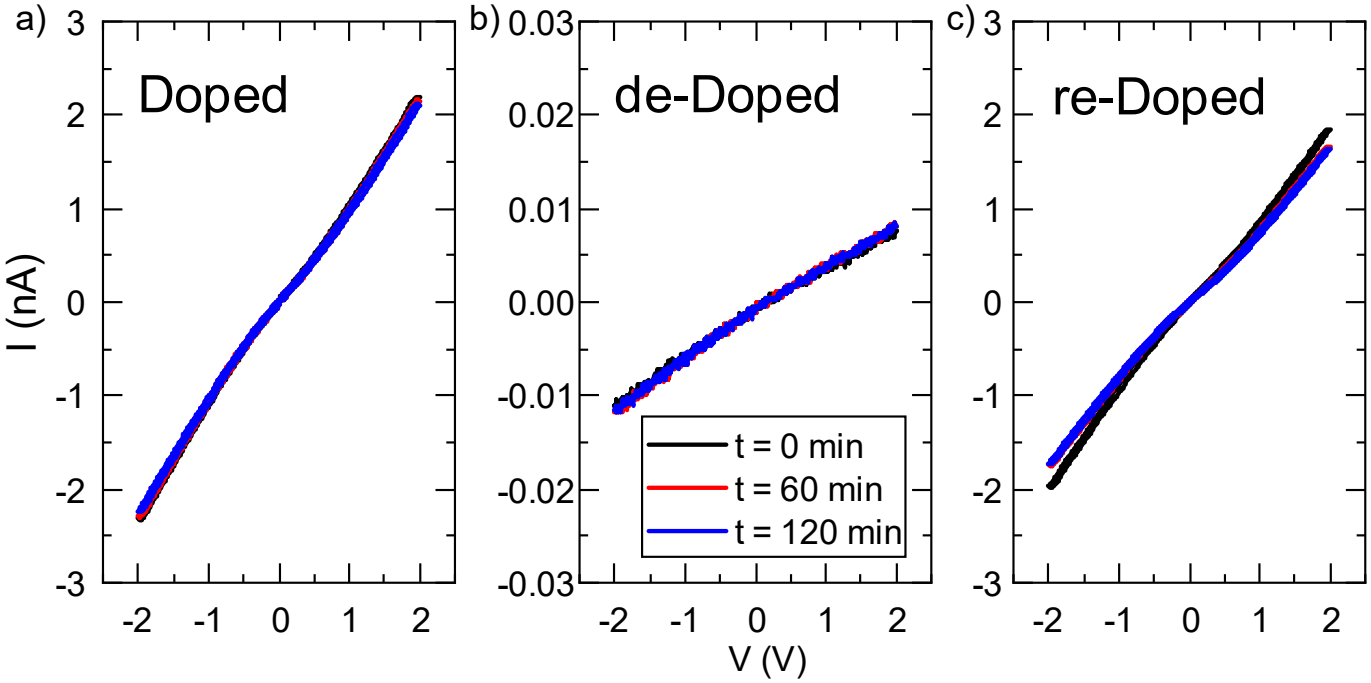


**Figure 3** *Current/voltage curves for a single P3HT nanowire after doping a), after de-doping b) and after re-doping c). The time estimated show that the sample is protected by a $N_2$ glovebag and the wires are not also doped with $O_2$ over the course of the measurements.*

and the surface potential distribution with Kelvin probe force microscopy (KPFM). To prevent the nanowire from oxidizing in air during the measurement, the entire measuring system was placed inside of a plastic glovebag with constant $N_2$ flow. The electrical current of the nanowire device in different doping conditions was measured with a current preamplifier (DL Instruments, model 1211) as source-drain bias ($V_{ds}$) was scanned. Figure 3 shows the I-V curves taken from a nanowire device after sequential doping with AN:F4TCNQ solution, de-doping with n-butylamine:acetone, and redoping from an AN:F4TCNQ solution, respectively. We previously demonstrated that immersion in a 1-aminobutane solution quantitatively removes F4TCNQ from conjugated polymer films.[8] The sequentially doped and re-doped P3HT/F4TCNQ samples have an I-V slope (conductance $G$) of 1.1 nS and 1.0 nS, while the de-doped wire has a conductance of only 0.005 nS, which shows that the wire can be reversibly doped and achieve its original performance. Each plot shows three curves measured directly after the sample was dried in vacuum and 60 and 120 minutes after the first measurement. Only in the re-doped sample are there any noticeable changes in the IV curve relative to the measurement time. The reproducibility of the IV curve for the doped and de-doped samples indicates that the glovebag and flow to minimize the introduction if atmospheric $O_2$ and $H_2O$ into our experimental setup and prevent secondary reaction of the OSC or dopant with atmospheric molecules. The nanowire has a thickness of ~20 nm, a width of 800-900 nm and length ($l$) of 40 $\mu m$ yielding a cross sectional area (A) of 16000 $nm^2$ and a doped conductivity $\sigma = \frac{G \cdot l}{A}$ of 0.034 S/cm and de-doped conductivity of $1.6 \times 10^{-4}$ S/cm.

Supporting information Figure S6 shows AFM and KPFM images of the same nanowire with $V_{ds}$ of 0 V and 2 V when the nanowire is doped (a, d, g), de-doped (b, e, h) and re-doped (c, f, i). Cross-sectional profiles of the KPFM images along the nanowire axis (j, k, l) shows a uniform potential drop along the nanowire, indicating that the doping of P3HT is uniform along the nanowire. Note that the sudden potential drop at $x = 20$ $\mu$m is an artifact caused by the fringe effect from the unremoved P3HT thin films nearby. The uniform potential drop along the nanowire also indicates that domain formation in the P3HT wire does not cause potential drops. This indicates that even confined to a wire with dimensions 10s-100s nm, the polymer P3HT with crystalline domains of 1s-100s nm can be treated as a uniform material. A small potential drop occurs near the metal contact, which is caused by the induced change in the barrier height at the polymer/metal junction.

Comparing to previous measurements of sheet resistance using a four wire-probe of sequentially doped P3HT film with a solution of F4TCNQ in acetonitrile with a concentration of 0.1 mol/L yields a doping level of ~2 mol% and conductivity of ~0.1 S/cm.[7] Since the ratio of polarons to neutral states in Figure 1 and SI Figure S6 is also very similar to the doping ratio published previously, we can conclude that the P3HT nanowire has approximately 3× lower conductiv-

ity for the same doping level as previously reported.[7] We can explain this difference by the thickness loss. In the previously published work the layer thickness was ∼50-60 nm before and after doping.[7] In the current paper, the thickness was ∼50 nm before doping but reduced to ∼20 nm during patterning of the wire as explained above. Thus the loss in conductivity is directly proportional to the loss in thickness. Other groups have reported increased conductivity in thinner P3HT films but in that case the film started thinner and no material was removed.[38] We also note that in previous measurements of P3HT/F4TCNQ samples, when a high potential is applied, the $F4TCNQ^-$ ions drift in the electric field and therefore move during a conductivity measurement.[39] The electric field applied here is far lower. We have no evidence that the distribution of $F4TCNQ^-$ ions changed during our measurements. Comparing to previous measurements of undoped P3HT films, Pingel et. al. reported a conductivity of $2\times10^{-}3$ S/cm using admittance measurements, which is approximately one order of magnitude higher than the $1.6 \times 10^{-4}$ S/cm reported here.[28] The Pingel paper reports a 100 nm thickness while we measured only 20 nm, so the undoped conductivity of the P3HT sample reported here is, within measurement error, identical to previously reported results.

Taken together the presented results so far show the beginning of a rapid and robust photopatterning system. We show diffraction limited optical writing of nanowires. The thickness is controlled by the polymer layer thickness and the lateral dimensions are written with a rapid write speed of $<1\times10^{-4}$s per pixel. The wires can be reproducibly doped and de-doped from solution, allowing these materials to be used for electrochemical applications or simply as patterned intrinsic and doped semiconductor domains. We show doped wire $\sigma$ of 0.034 S/cm in this publication, but point out that $\sigma$ of >30 S/cm has been recorded for P3HT using other sequentially deposited dopants[40,41] and conductivity for doped PBTTT, which is chemically, structurally and energetically similar to P3HT, has reported $\sigma$ ∼1000 S/cm.[42,43] It is therefore reasonable to assert that the processing steps depicted here enable pattering of polymer wires with a conductivity approaching lightly doped inorganic semiconductors, considering that Si doped at $10^{20}$ has a p-type conductivity of ∼1000 S/cm.[44] The electronic properties of doped OSCs are appropriate for circuits with small dimensions in which the resistance losses over small distances are acceptable.

A final demonstration needed to enable optical writing of semiconducting polymer nano-circuits is the ability to photopattern the semiconductor into realistic wire patterns. Figure 4 show "L" and "T" junctions between nanowires to demonstrate our ability to pattern wires to any arbitrary circuit diagram. Notice that in the bend region of the "L", the wire's thickness is neither thicker or thinner than the adjacent wire. This is an important demonstration because an additive printing technique electrohydrodynamic nanowire printing layers materials and junctions are much thicker than the surrounding wires. In the ""T" image, we attempted to write very narrow wires with a width of only ∼300 nm. The image clearly shows that we achieved a wire width of <290 nm, which is sub-diffraction limited length scale ($\frac{\lambda}{n} = \frac{405}{1.4} = 289nm$). At such small dimensions, the wire is not perfectly uniform in its cross sectional area because the wire dimension is smaller that the reliable resolution of the confocal microscope. The inconsistencies in height and width are all far smaller that the write wavelength. Minute vibrations coming from external stimulus like doors closing, chair scraping, moving air are sufficient to cause these small variations. Figure 4c and 4d show cross sections of the AFM image along both the x- and y-dimensions of the image. The "L" shaped wire shows a FWHM width of ∼200 nm in both dimensions. For the "T" shaped wire, one cross section shows a 70 nm thick wire with FWHM width of 270 nm while the other cross section has a thickness of only 35 nm and FWHM width of 120 nm. These inconsistencies in the pattern quality come from not using the "right" equipment for the job. A low-end maskless lithography instrument or a projection photomask could yield a global write speed increase of $10^5$–$10^6$ and simultaneous improvement in resolution. We used the LSCM because we were unable to adjust the depth of field in our photolithography instruments at Davis or Stanford.

We now compare the photopatterning technique that we demonstrated here with all of the patterning methods reviewed above. Techniques relying on prefabrication of wires are not able to be used for printing circuits with arbitrary form factor because they are difficult to manipulate. All established wet coating techniques are limited by fluid dynamics to lateral domains of tens of $\mu m$. Techniques relying on pre-patterning a substrate are not scalable and cannot work for multi-layers. Chemical cross-linking techniques are abundant and quite good, but the materials prepared to cross-link rarely perform as well as the unaltered polymer and the time/effort/expense required to include cross-linking chemistry has limited the development of industrial products. By comparison, DISC photopatterning uses polymer "out of the bottle" and can be adapted to pattern both doped and intrinsic polymers.[36] Several publications have now demonstrated diffraction limited patterning with a variety of form factors. Comparing all of the techniques, only DISC photopatterning and electrohydrodynamic organic nanowire printing[22] were able to achieve reliable wire/circuit fabrication to the diffraction limit of ∼300 nm using non-chemically altered OSCs. Both techniques show the ability to pattern a variety of different doped and intrinsic polymers. The sequential doping and de-doping demonstrated here and previously[8,34] is also fully compatible with the mixed polymer/PEO materials used in electrohydrodynamic printing, suggesting that the additive extrusion and subtractive photo-writing techniques could be used in combination with sequential doping to fabricate complex circuits composed of multiple different polymers. So far electrohydrodynamic extrusion, introduced above, has been more successfully used to fabricate working circuit elements other than wires.[22] DISC photopatterning pro-

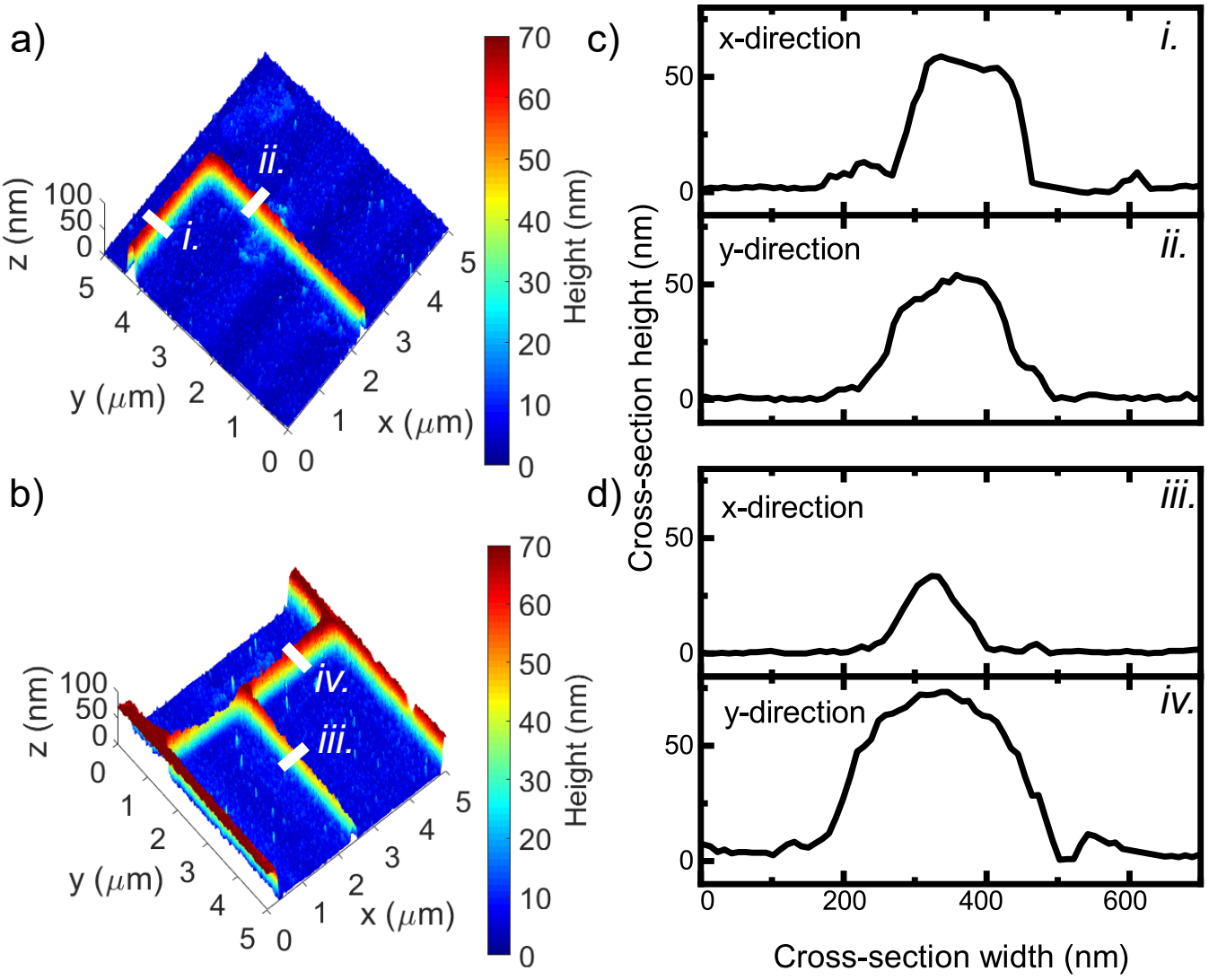


**Figure 4** *AFM images of P3HT nanowires: a) and d) show nanowires that were written in the form of a simple "L" bend and a "T", respectively. Images b) and c) show cross sections of the image in a) and e) and f) show cross section of the image in b). All cross sections show that the wire maintains a height of >50 nm and width of <500 nm.*

duces uniform controlled thickness at junctions, which is not possible with extruded wires.

DISC patterning is still a new idea and has not been engineered well yet. For example, our initial design for DISC patterning solvent cells was designed to be completely sealed in order to be allowed into a university user facility. Unfortunately, it took a long time (1 hr minimum) to remove the sample holder from the facility, move it to a different building with a glovebox, and then remove the tiny screws from the holder with gloves on. The result of this time delay in removing the sample from the solvent is that some of the P3HT and F4TCNQ that was heated and dissolved into the mTHF carrier solvent condenses back out of the solvent and can redeposit onto the substrate. This redeposition can be seen in Figure 2d as dark spots and in AFM Figures S6 and 4 as raised points on the blue background. Future research on DISC photopatterning should include design of optical patterning cells with flowing solvent that will prevent redeposition of removed P3HT material. Improved solvent cell design for rapid removal of the substrate (fewer screws) could save an hour for every substrate. The use of photolithography equipment that was designed for rapid photopatterning would result in a $10^5$ increase in patterning speed for the complete process because of high laser power, superior optics, and optimized rastoring of the laser. We demonstrated here the ability to controllably optically pattern conjugated polymer circuit elements with sub-$\mu m$ features using solution processing. We also identified relatively simple design improvements that yield the increase in processing speed necessary to make optical patterning using DISC a highly attractive technique for prototyping organic optoelectronic circuits.

# 4 Conclusions

Organic semiconductors already have desirable materials properties for optoelectronic devices with nanoscale dimensions. A review of patterning methods and the resulting application of these techniques to OSCs reveals that only nanopattern contact transfer printing, electrospinning of polymer filament mixtures through a nozzle, and dopant induced solubility control (DISC) photo patterning can reliably achieve sub-$\mu m$ printing of non-chemically altered OSC polymers. This article shows the first demonstration of DISC photo patterning in a simple device, a nanowire. We demonstrate direct–write subtractive photopatterning of P3HT/F4TCNQ wires with 200–900 nm width, 20–70 nm height, and 40 $\mu m$ length. Wires with form factors like "L" bends and "T" junctions are also demonstrated. The nanowire showed a maximum conductivity ($\sigma$) of 0.034 S/cm and Kelvin force prove measurements confirmed the uniform potential drop along the wire. This demonstrates that doped polymer nanowires can be rapidly optically patterned and achieve materials properties that are comparable to doped inorganic semiconductors. The ability to optically write any pattern down to diffraction limited resolution is a processing step that was missing in the organic electronics toolbox. This demonstration shows that OSC materials can now be tested and used in the full spectrum of optoelectronic devices that were not previously accessibly due to lack of an easy patterning methodology.

The main premise of DISC is that the solubility of a conjugated polymer can be greatly altered and controlled using molecular dopants like F4TCNQ. Here we again show that dopants can be reversibly added and removed using solution processing from high quality (high $M_W$ and regioregularity) P3HT films with no loss of thickness. However, lower quality (low $M_W$ and regio-regularity) P3HT is more soluble and results in film thickness loss during solvent processing. In addition, our previous work on high quality P3HT showed no change in crystal packing with sequential doping, whereas in this article we show that sequential doping does change the crystalline packing of the P3HT chains. We speculate that the different results come from some combination of lower quality P3HT having more defective crystals that allow some F4TCNQ intercalation and lower quality P3HT has a lower $T_g$. Since the $T_g$ of P3HT is near room temperature, expected variation in lab temperature and known variation in P3HT quality lead to different results with different processing history. These variations are important to document because they affect the electrical quality and reproducibility of OSC circuit elements. We therefore fabricated a nano-wire from a lower quality P3HT sample and compare the conductivity after fabrication, after chemical de-doping, and again after redoping. None of the samples show step changes in resistance, which shows that even when the wire diameter has dimensions approaching P3HT domains sizes, the wire performs electrically as a bulk material. The doped and re-doped samples have nearly identical conductivity, showing the sample loss can be controlled using pre-fractionation of the low quality P3HT.

# 5 Materials and methods

## 5.1 Materials

F4TCNQ (>98%) was purchased from TCI America. P3HT ($M_w$=54-75 kDa, >98% Regioregularity, Electronic grade, Batch # MKBV4158V), ($M_w$=50-75 kDa, >90% Regioregularity, Batch # MKCD1914), 2-Methyltetrahydrofuran anhydrous (mTHF), chlorobenzene (CB), acetonitrile anhydrous (AN), chloroform (CF), and Trichloro(octadecyl)silane (OTS) and all other solvents were purchased from Sigma-Aldrich. n-Hexane (97%) extra dry over molecular sieves was purchase from Acros Organics.

## 5.2 Substrates and home-built sample cell cleaning

30 mm round by 3.3 mm thick borosilicate substrates (Borofloat, Edmund Optics), 25 mm round #1 coverslips (Fisher Scientific) and one-inch native oxide silicon substrates were cleaned in an ultrasonic bath by 10 min sequential steps in acetone, methanol, isopropanol and DI water. After sonication, all substrates were blown dry with a nitrogen gun and placed in an UV-ozone-plasma cleaner for 30 min. The home-built sample cell and O-ring (McMaster-

Carr, 1108T13) were sonicated in acetone for 30 min and dried with nitrogen between measurements. All cleaned materials were transferred to a nitrogen glovebox (<3 ppm $H_2O$, $O_2$) for any further processing.

### 5.3 Gold electrodes deposition

Using an MBraun thermal evaporator, 5 nm of Cr (∼0.1 Å/s) followed by 95 nm of gold (∼1 Å/s) were deposited over the cleaned 25 mm round #1 coverslips through a deposition mask (Ossila, E292). Only the electrodes with channel lengths of 40 $\mu$m and 1 mm width (one per substrate) were used for conductivity measurements. After gold electrodes deposition the substrates were cleaned as previously described. See supporting information Figure S# for a microscope image of the gold electrodes.

### 5.4 Self-assembled monolayer (SAM)

200 $\mu$l of DI water was spin coated onto 25 mm round #1 coverslip with gold electrodes at 2500 rpm for 60 s. All traces of water were removed by blowing the substrate with nitrogen, then the substrate was transferred to a nitrogen glovebox. Under a nitrogen atmosphere, the substrate was soaked in a solution of n-Hexane:OTS:CF (1000:1:1, v/v) during 5 min. The substrate was removed from the deposition solution and transferred to another petri dish with 5 ml of n-Hexane for several seconds. The substrate was then placed on a spin coater and dynamically rinsed three times with 1 ml of CF at 1000 rpm for 60 s.

### 5.5 Film preparation

The thin films of P3HT were spin coated from a P3HT solution in CB (10 mg/ml,60 °C) at 1000 rpm for 60 s, producing films of 50±2 nm thickness. The films were sequentially doped from 0.1 mg ml$^{-1}$ F4TCNQ in AN at 1000 rpm. The doped film for patterning and conductivity measurements were dynamically rinsed with pure AN on a spin coater prior to being sealed inside a home-built cell with mTHF. It the excess F4TCNQ is not removed with AN, the F4TCNQ will crystallize in the P3HT in the mTHF solution and later the P3HT film is full of pin holes. Thus to achieve high film-quality patterning, it is necessary to pattern at low doping density and to remove aggregates of F4TCNQ. For chemical de-doping, the doped films were soaked in a 1-aminobutane:acetone (1:10, v/v) solution for 15 min and then dried for several minutes in the glovebox. Re-doped films were sequentially doped from 0.1 mg ml$^{-1}$ F4TCNQ in AN at 1000 rpm.

For grazing incidence wide-angle X-ray scattering (GIWAXS) measurements, ∼300 nm thick P3HT films were prepared by spin coating over native silicon oxide a P3HT solution in CB (25 mg/ml, 60 °C) at 1000 rpm until dried, and sequentially doped from 0.1 mg ml$^{-1}$ F4TCNQ in AN on a spin coater. The excess of doping solution was spinned off at 1000 rpm after leaving the film wet with An/F4TCNQ doping solution for 10 s.

### 5.6 Patterning and Imaging

The sealed P3HT doped film inside a home-built cell with mTHF was patterned on an Olympus FV1000 inverted microscope using a 60x objective. For patterning and imaging, a diode source of 405 nm and HeNe source of 543 nm were used, respectively.[6] To obtain a patterned P3HT doped wire, all the surrounded areas were fully removed along the channel by using the diode source at ∼166 $\mu$W with 200 $\mu s$ per pixel dwell time. The same procedure and patterned conditions were use to create "L" and "T" features.

### 5.7 Characterization

UV/vis/NIR spectra were measured using a PekinElmer Lambda 750 spectrometer. The wire UV/vis/NIR spectra (Figures 1 and S5) were collected under nitrogen, sealing the sample inside the glovebox in a home-built sample cell and avoiding air exposure during the dope, de-dope and redoping wire processing steps under study. Atomic force microscopy images from Figures 4, S3, and S4 were acquired in tapping mode on a Veeco Multimode Nanoscope IIIa AFM. The scan area was 40 $\mu$m by 20 $\mu$m, with a resolution of 6.4 pixels/$\mu$m and a scan rate of 7.8 ms/pixel. The wire current-voltage measurements were obtained under nitrogen atmosphere by a current preamplifier (DL Instruments, model 1211). The source-drain voltage was scanned between -2 V and 2 V, with a constant scan rate of 0.2 V/s.

Samples for X-ray scattering were spun-cast on native oxide Silicon substrates at UC Davis and immediately after driven to SSRL (Menlo Park, CA) for GIWAXS measurements. The time between sample preparation and measurement is estimated to be between 3 to 4 hours. GIWAXS was performed at the Stanford Synchrotron Radiation Lightsource (SSRL) on beam line 11-3 using an area detector (Rayonix MAR-225) and incident energy of 12.73 keV. The incidence angle of the beam (0.1°) was slightly larger than the critical angle, ensuring that we sampled the full depth of the film. The distance between sample and detector was calibrated using a LaB6 polycrystalline standard. X-ray measurements were performed in a Helium environment to minimize air scattering and beam damage to samples. Raw data was reduced and analyzed using Igor Pro and Nika data reduction software package.[45]

## Conflicts of interest

There are no conflicts to declare.

## Acknowledgements

This work was funded by the National Science Foundation Scalable Nanomanufacturing Program, Award # CMMI 1636385. R. X. and D. Y. acknowledge the U.S. National Science Foundation Grant DMR-1710737 for KPFM. Z.I.B.-V. acknowledges the SENER-CONACyT program for salary, Project # 291145. Confocal writing was performed at the Keck Spectral Imaging Facility at UC Davis. GIWAXS measurements were carried out at the Stanford Synchrotron Radiation Lightsource, a national user facility operated by

Stanford University on behalf of the U.S. Department of Energy, Office of Basic Energy Sciences. A.S.F. thanks the Wasson Honors Program for undergraduate research.

## Notes and references


[1] E. Menard, M. A. Meitl, Y. G. Sun, J. U. Park, D. J. L. Shir, Y. S. Nam, S. Jeon and J. A. Rogers, *Chemical Reviews*, 2007, **107**, 1117–1160.

[2] M. M. Ling and Z. N. Bao, *Chemistry of Materials*, 2004, **16**, 4824–4840.

[3] H. E. Katz, *Chemistry of Materials*, 2004, **16**, 4748–4756.

[4] B. Lüssem, C.-M. Keum, D. Kasemann, B. Naab, Z. Bao and K. Leo, *Chemical reviews*, 2016, **116**, 13714–13751.

[5] J. S. Chang, A. F. Facchetti and R. Reuss, *IEEE Journal on Emerging and Selected Topics in Circuits and Systems*, 2017, **7**, 7–26.

[6] I. E. Jacobs, E. W. Aasen, D. Nowak, J. Li, W. Morrison, J. D. Roehling, M. P. Augustine and A. J. Moule, *Advanced Materials*, 2017, **29**, 1603221.

[7] I. E. Jacobs, J. Li, E. W. Aasen, J. Lopez, T. Fonseca, G. Zhang, P. Stroeve, M. P. Augustine, M. Mascal and A. J. Moule, *Journal of Materials Chemistry C*, 2016, **4**, 3454–3466.

[8] I. E. Jacobs, F. Wang, N. Hazefi, C. Medina-Plaze, T. F. Harrelson, J. Li, M. P. Augustine, M. Mascal and A. J. Moule, *Chemistry of Materials*, 2017, **29**, 832–841.

[9] J. Rivnay, S. Inal, A. Salleo, R. M. Owens, M. Berggren and G. G. Malliaras, *Nature Reviews Materials*, 2018, **3**, 17086.

[10] J. Rivnay, R. M. Owens and G. G. Malliaras, *Chemistry of Materials*, 2014, **26**, 679–685.

[11] S. Khan, L. Lorenzelli and R. S. Dahiya, *Ieee Sensors Journal*, 2015, **15**, 3164–3185.

[12] D. D. Li, W. Y. Lai, Y. Z. Zhang and W. Huang, *Advanced Materials*, 2018, **30**, 1704738.

[13] K. Fukuda and T. Someya, *Advanced Materials*, 2017, **29**, 1602736.

[14] J. Bae, J. Lee, Q. Zhou and T. Kim, *Advanced Materials*, 2019, **31**, 1804953.

[15] D. Qin, Y. Xia and G. M. Whitesides, *Nat. Protocols*, 2010, **5**, 491–502.

[16] S. Y. Min, T. S. Kim, Y. Lee, H. Cho, W. Xu and T. W. Lee, *Small*, 2015, **11**, 45–62.

[17] S. Agbolaghi and S. Zenoozi, *Organic Electronics*, 2017, **51**, 362–403.

[18] A. C. Arias, J. D. MacKenzie, I. McCulloch, J. Rivnay and A. Salleo, *Chemical Reviews*, 2010, **110**, 3–24.

[19] R. Chesterfield, A. Johnson, C. Lang, M. Stainer, and J. Ziebarth, *Information Display*, 2011, 24–30.

[20] S. Gong and W. L. Cheng, *Advanced Electronic Materials*, 2017, **3**, 1600314.

[21] D. Ye, Y. J. Ding, Y. Q. Duan, J. T. Su, Z. P. Yin and Y. A. Huang, *Small*, 2018, **14**, 1703521.

[22] S.-Y. Min, T.-S. Kim, B. J. Kim, H. Cho, Y.-Y. Noh, H. Yang, J. H. Cho and T.-W. Lee, *Nature Communications*, 2013, **4**, 1773.

[23] J. Freudenberg, D. Jänsch, F. Hinkel and U. H. F. Bunz, *Chemical Reviews*, 2018, **118**, 5598–5689.

[24] M. C. Gather, A. Köhnen, A. Falcou, H. Becker and K. Meerholz, *Advanced Functional Materials*, 2007, **17**, 191–200.

[25] A. A. Zakhidov, J.-K. Lee, J. A. DeFranco, H. H. Fong, P. G. Taylor, M. Chatzichristidi, C. K. Ober and G. G. Malliaras, *Chemical Science*, 2011, **2**, 1178–1182.

[26] H. H. Fong, J.-K. Lee, Y.-F. Lim, A. A. Zakhidov, W. W. H. Wong, A. B. Holmes, C. K. Ober and G. G. Malliaras, *Advanced Materials*, 2011, **23**, 735–+.

[27] D. T. Scholes, P. Y. Yee, J. R. Lindemuth, H. Kang, J. Onorato, R. Ghosh, C. K. Luscombe, F. C. Spano, S. H. Tolbert and B. J. Schwartz, *Advanced Functional Materials*, 2017, **27**, 1702654.

[28] P. Pingel and D. Neher, *Physical Review B*, 2013, **87**, 115209.

[29] E. Lim, A. M. Glaudell, R. Miller and M. L. Chabinyc, *Advanced Electronic Materials*, 2019, **5**, 1800915.

[30] A. R. Chew, R. Ghosh, Z. R. Shang, F. C. Spano and A. Salleo, *Journal of Physical Chemistry Letters*, 2017, **8**, 4974–4980.

[31] C. Müller, *Chemistry of Materials*, 2015, **27**, 2740–2754.

[32] S. E. Root, S. Savagatrup, A. D. Printz, D. Rodriquez and D. J. Lipomi, *Chemical Reviews*, 2017, **117**, 6467–6499.

[33] F. P. V. Koch, J. Rivnay, S. Foster, C. Muller, J. M. Downing, E. Buchaca-Domingo, P. Westacott, L. Y. Yu, M. J. Yuan, M. Baklar, Z. P. Fei, C. Luscombe, M. A. McLachlan, M. Heeney, G. Rumbles, C. Silva, A. Salleo, J. Nelson, P. Smith and N. Stingelin, *Progress in Polymer Science*, 2013, **38**, 1978–1989.

[34] I. E. Jacobs, J. Li, S. L. Berg, D. J. Bilsky, B. T. Rotondo, M. P. Augustine, P. Stroeve and A. J. Moule, *ACS Nano*, 2015, **9**, 1905–1912.

[35] J. Fuzell, I. E. Jacobs, A. Ackling, T. F. Harrelson, D. M. Huang, D. S. Larsen and A. J. Moule, *Journal of Physical Chemistry Letters*, 2016, **7**, 4297–4303.

[36] Z. Su, Z. I. Bedolla-Valdez, L. Wang, Y. Rho, S. Chen, G. Gonel, E. N. Taurone, A. J. Moulé and C. P. Grigoropoulos, *ACS Applied Materials & Interfaces*, 2019, **11**, 41717–41725.

[37] J. Li, D. M. Holm, S. Guda, B.-V. Z. I., G. G., I. E. Jacobs, M. A. Dettmann, J. Saska, M. Mascal and A. J. Moule, *Journal of Materials Chemistry C*, 2019, **7**, 302–313.

[38] Y. Karpov, N. Kiriy, P. Formanek, J. Zessin, M. Hambsch, S. C. B. Mannsfeld, F. Lissel, T. Beryozkina, V. Bakulev, B. Voit and A. Kiriy, *ACS Applied Materials & Interfaces*, 2019, **11**, 4159–4168.

[39] L. Müller, S.-Y. Rhim, V. Sivanesan, D. Wang, S. Hietzschold, P. Reiser, E. Mankel, S. Beck, S. Barlow, S. R. Marder, A. Pucci, W. Kowalsky and R. Lovrincic, *Advanced Materials*, 2017, **29**, 1701466.

[40] C. Y. Kao, B. Lee, L. S. Wielunski, M. Heeney, I. McCulloch, E. Garfunkel, L. C. Feldman and V. Podzorov, *Advanced Functional Materials*, 2009, **19**, 1906–1911.

[41] A. I. Hofmann, R. Kroon, S. Zokaei, E. Järsvall, C. Malacrida, S. Ludwigs, T. Biskup and C. Müller, *Under review*.

[42] K. Kang, S. Watanabe, K. Broch, A. Sepe, A. Brown, I. Nasrallah, M. Nikolka, Z. Fei, M. Heeney, D. Matsumoto, K. Marumoto, H. Tanaka, S. Kuroda and H. Sirringhaus, *Nat Mater*, 2016, **15**, 896–902.

[43] Y. Yamashita, J. Tsurumi, M. Ohno, R. Fujimoto, S. Kumagai, T. Kurosawa, T. Okamoto, J. Takeya and S. Watanabe, *Nature*, 2019, **572**, 634–638.

[44] A. Rockett, *The Materials Science of Semiconductors*, Springer, 2008.

[45] J. Ilavsky, *J. Appl. Cryst.*, 2012, **45**, 324–328.